Korean J. Chem. Eng., 36(12), 2074-2084 (2019)
DOI: 10.1007/s11814-019-0372-1

pISSN: 0256-1115
eISSN: 1975-7220

Hydrodynamic modeling of the spiral-wound membrane module including the membrane curvature: reverse osmosis case study

Morteza Taherinejad, Mahdi Moghimi†, and Shahram Derakhshan

School of Mechanical Engineering, Iran University of Science and Technology, Tehran, Iran
(*Received 5 June 2019 • accepted 22 August 2019*)

Abstract−This study presents an integrated analytical model for the hydrodynamic behavior of the spiral-wound membrane element considering the curvature of the flow feed and permeate channels. The new model introduces a set of closed-form expressions for the output parameters of the permeate flow rate, fluid recovery fraction, and the permeation flux, which can be a necessary tool for optimization and evaluation of the parameters involved in the problem. Accordingly, the results were set forth for a reverse osmosis water treatment SWM element. The difference in the output parameters for the solutions with flat and curved membranes was investigated, and the consequences of the common assumption of the flat-sheet membrane were examined mathematically. It was found that neglecting the membrane curvature implements a significant impact/error on the prediction of the permeate channel pressure and membrane width with maximum permeation rate, whereas its impacts on feed channel pressure and output parameters are insignificant, especially for the considered reverse osmosis case study. Also, the curvature effect on the solution can be magnified by three parameters of the membrane width: permeate channel permeability, and membrane resistance.

Keywords: Hydrodynamics, Curvature, Spiral-wound Membrane Element, Water Permeate Flow Rate, Fluid Recovery Fraction

INTRODUCTION

Spiral-wound membrane (SWM) elements are used in a variety of applications, such as gas separation, dairy industry, post-combustion pollution control, and membrane-based water treatment processes including reverse osmosis (RO), nanofiltration (NF), ultrafiltration (UF), and microfiltration (MF). In water treatment, SWM elements are very common among the available membrane elements due to high area to volume ratio. In the SWM element, several layers of flat sheet membrane, feed channel mesh spacer and permeate channel collector medium are wound around the permeate collection tube to produce flow channels for permeate and feed fluid. Pressure-driven membrane processes, such as reverse osmosis, employ a pressure gradient between the feed and permeate sides as the driving force of the separation to pass solvent through the membrane. Accordingly, particles and solutes are separated based on size, shape, and charge [1]. Even though this process needs consumption of energy in pumps, at present reverse osmosis is the most energy-efficient technology for desalination and is the benchmark for comparison for any new desalination technology [2].

Understanding and modeling of the complex physics of spiral-wound membranes, especially for water treatment, have been the purpose of many studies, which have been reviewed in [3-5]. Presenting the models in order to express the system behavior [6,7], analyzing the geometric and operational conditions in order to decrease the fouling [8-10] and hydrodynamic simulation and introducing feed channel pressure drop correlations [11,12] are among the subjects to study various physical aspects of SWMs.

In this field, mathematical models are always noteworthy and have been used widely [7,13-15] for predicting the SWM hydrodynamic and mass transfer despite their simplifying assumptions. At all of these analytical and other numerical studies [11,16,17], for simplification, membrane curvature has been assumed negligible. This assumption is very common in the literature but its validity has been the subject of very few studies. For instance, about a decade ago, Ranade and Kumar [18] applied a three-dimensional CFD model to study the effect of curvature on the hydrodynamics of the SWM element feed channel. By the unit cell approach, various spacer configurations were examined, and the results showed that the flow fields were little different between curved and flat spaces when the spacer is present. This is because secondary flows caused by curvature are not significant compared with those generated by the spacer geometry.

Between 2009 and 2012, Li et al. [19-21] applied 2D [19,21] and 3D [20] CFD models with various spacer configurations to study the effect of curvature on the hydrodynamics and particle deposition. From the hydrodynamics, they showed that there is an imbalance of shear stress between the inner and outer feed channel walls because of the curvature. This would imply the different extents of fouling in the feed channel at different radial positions which results in the non-uniform performance between membrane leaves in the module [19]. They optimized the design of the feed channel spacer with an emphasis on the relative size of filaments between the inner and outer layers [20]. In their third study [21], particle deposition was found to be strongly affected by flow distribution, decreasing in areas of high shear stress. Spacers with zigzag and submerged configuration exhibited low curvature effect on particle deposition and led to less unequal deposition of the colloidal material on the

†To whom correspondence should be addressed.
E-mail: moghimi@iust.ac.ir

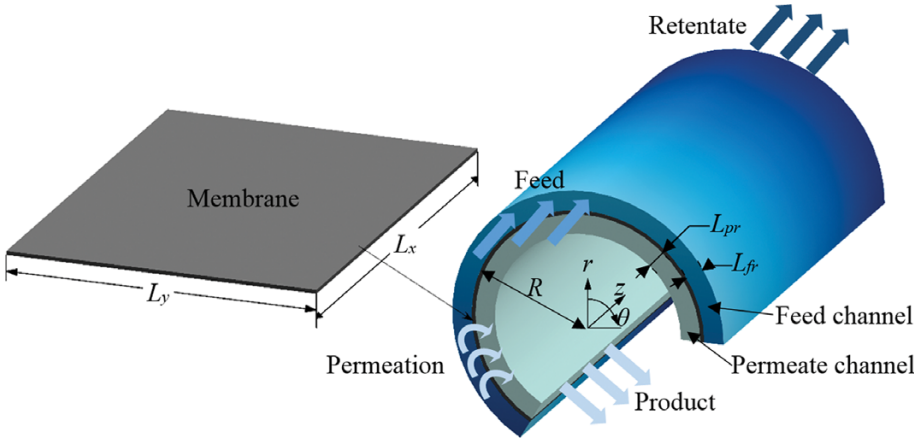

Fig. 1. The cylindrical solution geometry - curved feed and permeate channels.

inner and outer membranes. In 2009, Wardeh and Morvan [22] again used CFD to numerically determine detailed contours of pressure, wall shear stress, and mean salt accumulation on the membrane in the curved channel. In a more recent study, Tung et al. [23] considered the curved feed channel of UF and RO SWM elements to analyze the fouling distribution by means of both the ultrasound measurement system and the CFD. In agreement with what Le et al. [19-21] reported, the curvature affected the shear stress at inner and outer membranes, but was less significant in comparison to the shear stress induced by the gravity (for vertical element orientation) and spacers.

Although the effect of the surface curvature has been assessed in the literature at the aforementioned studies, an analytical model considering the curvature as a parameter, which is done in this study, has never been presented. A mathematical solution, even with its simplifications and assumptions, can cause to investigate the missed areas for enhancing the physical understanding of the problem dealt with. For example, previous CFD studies were mostly performed at the size scale of a unit cell (to decrease the computational costs) and only with some discrete limited number of the curvature levels. Or there was no argument about some physical properties that can magnify the effect of curvature. Besides, the effect of the curvature on the permeate side of the membrane is another uninvestigated area of this field. While in the presented integrated model, it is easy and fast to see the effect of curvature under a wide range of different conditions and in full scale of the membrane size. This would aware the researchers more efficient from the consequences of the flat membrane assumption.

At the author's previous study [7], a mathematical solution was presented for a flat feed and permeate channels with a membrane between connecting the two fluid flow domains. Now, the previous analytical model is developed considering a cylindrical SWM element with a constant radius. With the idea of expanding the two coupled flow equations for the feed and permeate channels in the cylindrical coordinates, the parameter of curvature radius was imported to the authors' previous model. It concludes the new pressure distribution for both channels that had not been presented before in any other analytical model. By the new presented model, more comprehensive analysis of curvature effects on an SWM element operational parameters like permeate flow rate, fluid recovery fraction and permeation flux is provided, and the difference between the solutions with and without curvature is studied. It is believed that a better understanding of the acceptation consequences of flat membrane assumption has arisen.

GEOMETRY

Fig. 1 shows the solution domain of the study. As shown, for developing the new mathematical model without flat sheet assumption, the fluid flow channels (feed and permeate channels) are considered as a cylindrical shell with the thickness equal to the height of the channel. The length of this shell along the *z*-direction is equal to the element/membrane length (L_x), and the perimeter at the shared edge of the two channels is equal to the membrane width (L_y). The membrane is wrapped in the direction of θ with the constant radius of R. The membrane thickness is not geometrically considered, meaning that the inner surface of the feed channel and the outer surface of the permeate channel are coincident at the radius of R. However, the physical effect of the membrane thickness is implemented in the solution as the concept of membrane resistance. The channels is at the direction of r which is L_{fr} at the feed side and L_{pr} at the permeate side of the membrane. The cylindrical coordinate of (r, θ, z) was used for both the feed and permeate channels fluid flow analysis.

In practice, when several membrane envelopes roll alongside each other around the permeate tube, the final geometry of the channels is spiral. Here, for simplification, the rolled membranes and the produced fluid flow spaces are considered as the cylindrical shell in which the angle corresponds to the width of the membrane (Θ) will be $\Theta=L_y/R$. The mainstream in feed channel flows at the direction of z and in permeate channel at the direction of θ. The product fluid is gathered at the end of the permeate channel at the center by the permeate tube.

GOVERNING EQUATIONS

The equations of the conservation of mass and momentum govern the hydrodynamics of fluid flow in spiral-wound membranes

that are discussed in various references [14,24]. In the following, the governing equations will be discussed and the pressure equations for fluid channels will be derived from these governing equations.

1. Derivation of Pressure Equation for the Permeate Channel

In the permeate side of the membrane, there is a permeate spacer (also known as permeate carrier or tricot) that is a porous material with small apertures much smaller than the channel thickness. The permeate spacer is a polyester fabric with the ability to quickly whisk water away from the membrane. In this channel, the velocities are very small and the Darcy equation can be used. An anisotropic porous medium is considered with the permeability of k_1 in the parallel direction of the membrane (θ and z) and the permeability of k_2 in the direction perpendicular to the membrane (r). Therefore, from the linear Darcy equation the components of the velocity vector $\overrightarrow{U_P}=(u_r, u_\theta, u_z)$ in the permeate channel would be:

$$u_r=-\frac{k_2}{\mu}\frac{\partial P}{\partial r} \tag{1}$$

$$u_\theta=-\frac{k_1}{\mu r}\frac{\partial P}{\partial \theta} \tag{2}$$

$$u_z=-\frac{k_1}{\mu}\frac{\partial P}{\partial z} \tag{3}$$

where P is the pressure of the permeate channel.

From the mass continuity equation for incompressible flow ($\nabla\cdot\overrightarrow{U_P}=0$) and the velocity components from Eqs. (1), (2) and (3), the combination of Darcy momentum equation and mass continuity equation will reach a differential pressure equation as:

$$\frac{k_2}{k_1}\frac{1}{r}\frac{\partial}{\partial r}\left(r\frac{\partial P}{\partial r}\right)+\frac{1}{r^2}\frac{\partial^2 P}{\partial \theta^2}+\frac{\partial^2 P}{\partial z^2}=0 \tag{4}$$

The solution domain of the Eq. (4) will be in the range of $(R-L_{pr})<r<R$, $0<\theta<\Theta$, and $0<z<L_x$.

In this fluid domain, there is no flow at the two sides of *z*-axis (two longitudinal sides of the element) and also no flow at the intersection of the channel and outer element shell. All the entered fluids go out of the channel from only one side in contact with the permeate tube with constant outlet pressure. In the direction of r, one side is blocked where is no membrane and at the other side where the membrane is located, the flow is coming into the channel with the velocity value of permeation velocity (U_w). All of these situations are expressed mathematically as:

$$r=R-L_{pr}:\frac{\partial P}{\partial r}=0,\ r=R:\frac{\partial P}{\partial r}=-\frac{\mu}{k_2}U_w \tag{5}$$

$$\theta=0:P=P_{out},\ \theta=\Theta:\frac{\partial P}{\partial \theta}=0 \tag{6}$$

$$z=0,\ z=L_x:\frac{\partial P}{\partial z}=0 \tag{7}$$

Eq. (4) is presented to obtain a three-dimensional pressure distribution, but with regard to the geometry of the flow, the channel pressure variations along the *r*-axis are negligible. Therefore, the permeate channel pressure can be in the form of $P(\theta, z)$. To remove the first term of Eq. (4), this equation is averaged along the radial direction as follows:

$$Eq(\theta,z)=0:\frac{1}{A}\int Eq(r,\theta,z)dA=\frac{\int_{r=R-K_{pr}}^{R} Eq(r,\theta,z)(2\pi r dr)}{\pi(R^2-(R-L_{pr})^2)}=0 \tag{8}$$

where this process is performed using two boundary conditions of Eq. (5) on the upper and lower walls of the permeate channel. The parameter of permeation velocity (U_w), which exists in the Eq. (5), includes the membrane intrinsic properties and provides a connection between the pressure fields of two sides of the membrane with this equation [7,14]:

$$U_w=\frac{1}{\mu R_m}(p-P) \tag{9}$$

where the R_m indicates the membrane resistance (the ratio of membrane thickness to membrane permeability), μ is the viscosity and p is the feed channel pressure on the membrane surface.

Finally, the integrating process of Eq. (8) from Eq. (4) with implementing the conditions of Eqs. (5) to (7), leads to the pressure equation for permeate channel as:

$$\frac{2\ln\left(\frac{R}{R-L_{pr}}\right)}{R^2-(R-L_{pr})^2}\frac{\partial^2 P}{\partial \theta^2}+\frac{\partial^2 P}{\partial z^2}=\frac{2R}{(R^2-(R-L_{pr})^2)k_1 R_m}(P-p) \tag{10}$$

Note that when $R\to\infty$, Eq. (10) is converted into Eq. (11), which was obtained by assuming the flat sheet membrane in the previous study [7].

$$\frac{\partial^2 P}{\partial x^2}+\frac{\partial^2 P}{\partial y^2}=\frac{1}{k_1 R_m L_{pz}}(P-p) \tag{11}$$

2. Derivation of Pressure Equation for the Feed Channel

In the feed channel, as in the permeate channel, the Darcy pressure drop equation is used to avoid the complexities of mathematically solving the full Navier-Stokes equations. This complexity relates to the different aspects same as partial differential non-linear intrinsic of the Navier-Stokes equations and also the geometry complexity made by the presence of the spacer in this channel.

In the proposed mathematical model, the effects of the spacer with different configurations and geometries are considered by using the permeability of the fluid domain as a function of Reynolds number, which is a way for jumping from the geometry complexities [25]. Therefore, the relationship between the pressure drop and the velocity in this channel is expressed as:

$$\frac{\Delta p}{\Delta L}=-f_1 Re^{-f_2}\frac{U^2\rho}{D} \tag{12}$$

Note that the geometric and functional effects of the spacer are expressed by two parameters of f_1 and f_2, which are obtained from CFD in several studies [26,27]. The Reynolds number is commonly defined as $Re=\rho UD/\mu$ where the spacer filament diameter D and the superficial velocity U (based on the empty channel) are used as the characteristic length and velocity, respectively.

Eq. (12) can be used in three directions, so it can be rewritten in vector form as:

$$\vec{U}=\frac{D^{1+f_2}}{f_1 U^{1-f_2}\rho^{1-f_2}\mu^{f_2}}\nabla p \tag{13}$$

where the magnitude of the velocity vector $\vec{U}=(U_r, U_\theta, U_z)$ is ob-

tained as:

$$U=\left(\frac{D^{1+f_2}}{f_1\rho^{1-f_2}\mu^{f_2}}|\nabla p|\right)^{1/(2-f_2)} \tag{14}$$

By applying a local mass balance for an element with the differential length along the *z*-axis and the height along the *r*-axis equal to channel height, similar to what was done by Kostoglou and Karabelas [28], and substituting the Eq. (13) for velocity vector and Eq. (14) for the magnitude of the velocity in the mass equation, the pressure equation for the feed channel is obtained as follows:

$$|\nabla p|^{(f_2-1)/(2-f_2)}(\nabla\cdot\nabla p)=\left(\frac{f_1\rho^{1-f_2}\mu^{f_2}}{D^{1+f_2}}\right)^{1+(f_2-1)/(2-f_2)}\frac{1}{\mu R_m L_{fr}}(p-P) \tag{15}$$

The solution domain of the Eq. (15) will be in the range of $R<r<(R+L_{fr})$, $0<\theta<\Theta$ and $0<z<L_x$. The boundary conditions for the six faces of this channel are considered as:

$$\begin{aligned}&r=R+L_{fr}: U_r=U_\theta=U_z=0,\ r=R: U_r=-U_w,\ U_\theta=U_z=0\\&\theta=0,\ \theta=\Theta: U_r=U_\theta=U_z=0\\&z=0: p=p_{in},\ z=L_x: p=p_{out}\end{aligned} \tag{16}$$

3. Dimensionless Equations

As discussed in the two previous sections, the pressure equations are presented as Eq. (10) for permeate channel and Eq. (15) for feed channel. Here, it is assumed that the pressure varies only in z and θ direction for both flow channels (by averaging for permeate channel and considering the negligible variation for feed channel along the direction of r). This assumption has been validated by Kostoglou and Karabelas [14].

The dimensionless variables are denoted by the subscript "d". All the length variables are normalized with the element/membrane width L_y, the angles with the angle corresponding to the membrane width Θ, and the pressures with the operating pressure (p_{in}) so $p_{od}=p_{out}/p_{in}$.

Finally, by normalizing the two aforementioned main pressure equations for two channels, the new partial differential dimensionless equations are obtained as follows:

$$\left[\left(\left(\frac{\partial p_d}{\partial\theta_d}\right)^2+\left(\frac{\partial p_d}{\partial z_d}\right)^2\right)^{\frac{1}{2}}\right]^{\alpha}\left(\frac{\partial^2 p_d}{\partial\theta_d^2}+\frac{\partial^2 p_d}{\partial z_d^2}\right)=A(p_d-P_d) \tag{17}$$

$$\frac{\partial^2 P_d}{\partial\theta_d^2}+C\frac{\partial^2 P_d}{\partial z_d^2}=B(P_d-p_d) \tag{18}$$

with the boundary conditions of:

$$\begin{aligned}&z_d=0: \frac{\partial P_d}{\partial z_d}=0,\ p_d=1\\&z_d=L_{xd}: \frac{\partial P_d}{\partial z_d}=0,\ p_d=p_{od}\\&\theta_d=0: P_d=0,\ \frac{\partial p_d}{\partial\theta_d}=0\\&\theta_d=1: \frac{\partial P_d}{\partial\theta_d}=0,\ \frac{\partial p_d}{\partial\theta_d}=0\end{aligned} \tag{19}$$

The dimensionless variables of α, A, B, and C appearing in the problem are given as:

$$\alpha=\frac{f_2-1}{2-f_2} \tag{20}$$

$$A=\left(\frac{f_1\rho^{1-f_2}\mu^{f_2}}{D^{1+f_2}}\right)^{1/(2-f_2)}(R\,\Theta)^{2+(f_2-1)/(2-f_2)}\frac{P_{in}^{(1-f_2)/(2-f_2)}}{\mu R_m L_{pr}} \tag{21}$$

$$B=\frac{R\,\Theta^2}{\ln\left(\frac{R}{R-L_{pr}}\right)k_1 R_m} \tag{22}$$

$$C=\frac{R^2-(R-L_{pr})^2}{2R^2\ln\left(\frac{R}{R-L_{pr}}\right)} \tag{23}$$

As can be seen in the dimensionless variables introduced in Eqs. (20) to (23), the fluid properties of viscosity and density are included in these variables that can affect the solution. Although these parameters can be the function of the concentration in reality, since the mass transfer phenomenon has not been considered in this study, these parameters are assumed constant or, in other words, the fluid is considered the pure and single phase.

4. Solution Method

Here, to solve the normalized equations of (17) and (18), a hypothesis called "1+1 directions" is used to simplify the equations and obtain the distribution of pressure in two channels of feed and permeate. This assumption means that the main direction of flow is along the length of the membrane/element in the feed channel and along the membrane width in the permeate channel, and thus the flow parameters variation would be in these directions. This assumption is relevant in membrane/meso scale models [29, 30] and its validity has been examined and confirmed by Kostoglou and Karabelas [14]. Using this assumption, the dimensionless parameter of C in the permeate channel pressure equation is omitted from the parameters circle. In addition, it has also been shown [14] that when the flow velocity in the feed channel is low, the governing equation in the feed channel is the Darcy linear equation ($f_2=1$), in which case the α term would be zero. In the following, despite the coordination change and the presentation of new dimensionless parameters, the simplified dimensionless equations will be exactly the same as in previous study [7] with flat sheet membrane. Therefore, the solving process of Eqs. (17) and (18) will not change, and finally the distribution of dimensionless pressure $p_d(z_d)$ in the feed channel and $P_d(\theta_d)$ in the permeate channel would be as follows:

$$P_d(\theta_d)=C_1e^{\sqrt{B}\theta_d}+C_2e^{-\sqrt{B}\theta_d}-\frac{1}{2}\gamma L_{xd}+1 \tag{24}$$

$$p_d(z_d)=C_4e^{\sqrt{A}z_d}+C_5e^{-\sqrt{A}z_d}+C_3 \tag{25}$$

where the equations for coefficients of $C_{1..5}$ are:

$$\begin{aligned}C_1&=\frac{1}{2}\frac{e^{-\sqrt{B}}(\gamma L_{xd}-2)}{e^{\sqrt{B}}+e^{-\sqrt{B}}}\\C_2&=\frac{1}{2}\frac{e^{\sqrt{B}}(\gamma L_{xd}-2)}{e^{\sqrt{B}}+e^{-\sqrt{B}}}\\C_3&=-\frac{(-2+\gamma L_{xd})((-1+\sqrt{B})e^{2\sqrt{B}}+1+\sqrt{B})}{\sqrt{B}(2e^{2\sqrt{B}}+2)}\end{aligned} \tag{26}$$

$$C_4=\frac{(C_3-1)e^{-\sqrt{A}L_{xd}}-C_3+p_{od}}{e^{\sqrt{A}L_{xd}}-e^{-\sqrt{A}L_{xd}}}$$

$$C_5=\frac{(C_3-1)e^{\sqrt{A}L_{xd}}-C_3+p_{od}}{e^{\sqrt{A}L_{xd}}-e^{-\sqrt{A}L_{xd}}}$$

Note that the presented model prepares this opportunity to simply calculate the output parameters from the set of algebraic equations. There is no need to have the grid same as numerical methods, and also the curvature of the membrane was taken into account as a new parameter.

5. Output Parameters and the Case Study

Using the pressure distribution Eqs. (24) and (25) obtained from the solution, two important parameters of the fluid recovery fraction (F) and the permeate water flow rate (Q) are achievable from their definitional concept. The permeate water flow rate is the total volumetric flow rate of water permeating through the membrane, and fluid recovery fraction is a term used to describe the fraction of the inlet flow permeating through the membrane. Thus, the permeate water flow rate is calculated from $Q_{permeate}=(AU)_{in}-(AU)_{out}$ (the difference between the fluid flow rate at the inlet and the outlet of the feed channel), and the fluid recovery fraction is calculated from $F=Q_{permeate}/Q_{in}$ or simply $F=((AU)_{in}-(AU)_{out})/(AU)_{in}$. The velocities needed to calculate the output parameters can be obtained from Eq. (15) after the calculation of the feed channel pressure distribution from Eq. (25). Also, the mean permeation velocity (U_w), as the third output parameter analyzed in this study, can be calculated by dividing the permeate flow rate by the area of the membrane.

Here, to have an indicator of how much is the intensity of the channel curvature, the parameter of dimensionless curvature radius (η) is defined using the outer radius of the channel (R_o), the inner radius of the channel (R_i) and the average radius of the channel ($R_{ave}=(R_o+R_i)/2$) as follows:

$$\eta=\frac{R_o-R_i}{R_{ave}} \tag{27}$$

So, the dimensionless curvature radius can be obtained from the permeate channel information according to Fig. 1 as:

$$\eta=\frac{L_{pr}}{R-L_{pr}/2} \tag{28}$$

The mathematical range of dimensionless curvature radius is between 0 (minimum curvature) and 2 (maximum curvature), which η=0 indicates the flat sheet situation ($R\rightarrow\infty$) and η=2 corresponds to an unrealistic half-circle channel ($R=L_{pr}$). The range of dimensionless curvature radius for industrial water filtration elements has been reported from 0-0.061 to 0-0.165 for RO and from 0-0.052 and 0-0.182 for UF spiral-wound membranes [20].

To illustrate the difference of the presented solution and the solution with the flat-sheet assumption, the parameter of the "percentage of difference" ($\psi_q(\eta)$) for the desired parameter of q is defined as:

$$\psi_{q,\eta}=\frac{q|_{\eta}-q|_{\eta=0}}{q|_{\eta=0}}\times 100 \tag{29}$$

where the desired parameter of q can be either the product water flow rate, the fluid recovery fraction, or other output parameters.

To provide the results, there is a need for a basic case study with known geometric and operational conditions. Hence, the values for the first RO element (commercial Dow module BW30-400) of a common 7-element brackish water treatment arrangement in an 8-in pressure vessel are used which were referenced from Koutsou et al. [13]. This arrangement has the feed concentration of 2,000 mg/L TDS with the known input feed pressure and pressure drop. The total recovery fraction of the arrangement is 70% but the recovery fraction of 12% has been declared for the first element.

RESULTS AND DISCUSSION

1. The Point of Effect of the Curvature on the Final Equations and the Solution Validation

It is useful to investigate how the curvature parameter behaves

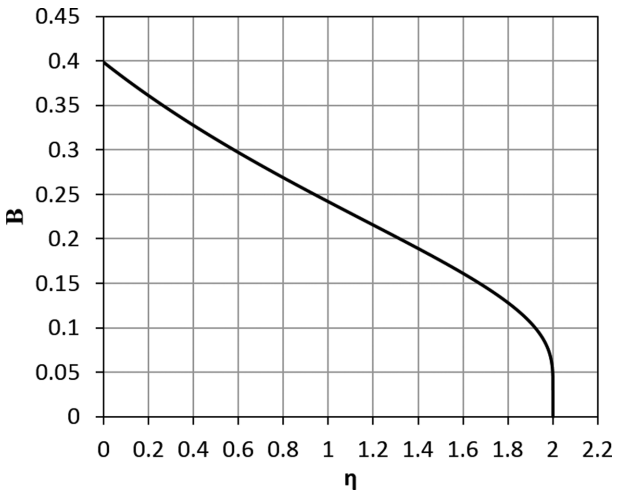

Fig. 2. Effect of dimensionless curvature radius η on dimensionless parameter of B.

Table 1. The case study RO SWM element design and operating parameters

Operating parameters	
Feed flow rate, Q	10 m^3/h
Total recovery fraction, F_{total}	70%
1st Element recovery fraction, F	12%
Inlet pressure, p_{in}	12.4 bar
Pressure drop, Δp	0.35 bar
Design parameters	
Membrane resistance, R_m	0.9×10^{14} m^{-1}
Total element membrane area	37.1 m^2
Number of envelopes	15
Membrane sheet length, L_x	0.96 m
Membrane sheet width, L_y	1.285 m
Feed side spacer geometry	L/D=8, β=90° (f_1=0.8, f_2=0.19) [26]
Spacer diameter, D	0.5 mm
Permeate side permeability, k_1	2×10^{-10} m^2
Feed channel gap, L_{fr}	0.71 mm
Permeate channel gap, L_{pr}	0.23 mm

Table 2. Comparison of the values of the output parameters

	ROSA data	Flat channel [7]	This study (η=0.061)	This study (η=0.165)
1st Element recovery fraction, F (%)	12	8.2	9.27	9.32
Total element permeate flow, Q (Lit/h) (*)	1230	1122	1126	1132
Permeate flux (LMH)	33.1	30.33	30.43	30.6
Dimensionless parameter B	---	0.3988	0.3869	0.3676

(*)=(each 0.96(m)×1.285(m) membrane flow rate)×(2 side membrane)×(15 envelopes)

in the final equations. With attention to the newly presented relations, the dimensionless parameter of B implements the curvature effect to the solution originally. Note that the parameter of B expresses the degree of influence of the flow in the permeate channel from the high-pressure flow field of the feed channel. Fig. 2 can be simply extracted from the definition of the B (Eq. (22)); it shows the dependence of B on the curvature. As can be seen, if the curvature radius of the SWM is infinite (flat plate), then B is about 0.4. As curvature increases, B is reduced, which means that greater curvature will lead to less effect of the feed channel on the permeate channel.

The modified value of B in the presented model can conclude a better prediction of important output parameters of the fluid recovery fraction (F), permeate flow rate (Q) and permeation flux (LMH). This fact is proved in Table 2. The case study used in Table 2 for comparison corresponds to the basic case study introduced in Table 1. In Table 2, the output parameters are obtained with the current model for two constant dimensionless curvature radii of 0.061 and 0.165, which are the highest values within the range of RO commercial elements. The results were compared with the flat-sheet membrane results of Taherinejad et al. [7] and the simulation results of the reverse osmosis system analysis (ROSA) software. ROSA software was developed by Dow Company based on empirical data generated by experimentally testing of Filmtec™ products, which presents highly reliable and validated results for RO modules [31]. As can be seen, although the variations of the output parameters are not significant (with these magnitudes of the curvature and other particular properties related to the RO case study), the new model suggests closer values in comparison with flat-sheet solution to the claimed values in the software of the membrane constructor (ROSA). The illustrated difference between the model results and ROSA results is not out of expectations despite all the simplifying assumptions made in the presented analytical model.

2. Effect of the Surface Curvature on the Pressure Distribution of the Two Flow Channels

The dimensionless pressure equations (Eqs. (24) and (25)) obtained from the development of the analytical solution are in fact the source of calculation and prediction of the hydrodynamic behavior of the SWM element. The dimensionless pressure distribution for the permeate channel is shown in Fig. 3. As is clear, the surface curvature has an impressive effect on the pressure distribution of the permeate channel. At the point θ_d=0, the relative pressure of the outlet is zero and, thus, the absolute pressure is equal to the pressure of the treated water in the permeate tube. Also, at the lateral end of the channel, the flow of water due to the channel closure is zero and the highest pressure is observed at this point. In-

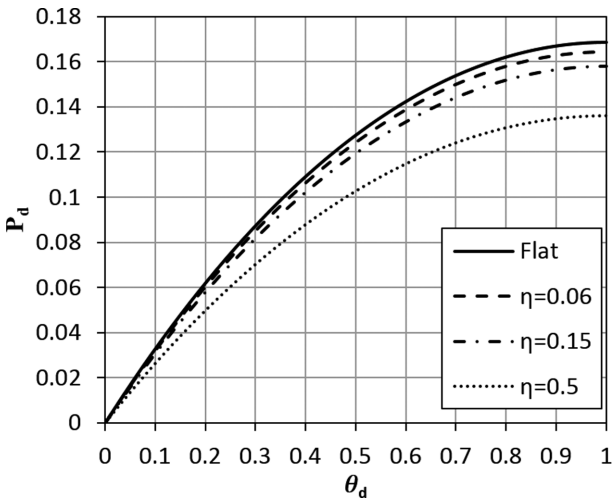

Fig. 3. Pressure distribution in permeate channel with different dimensionless curvature radii.

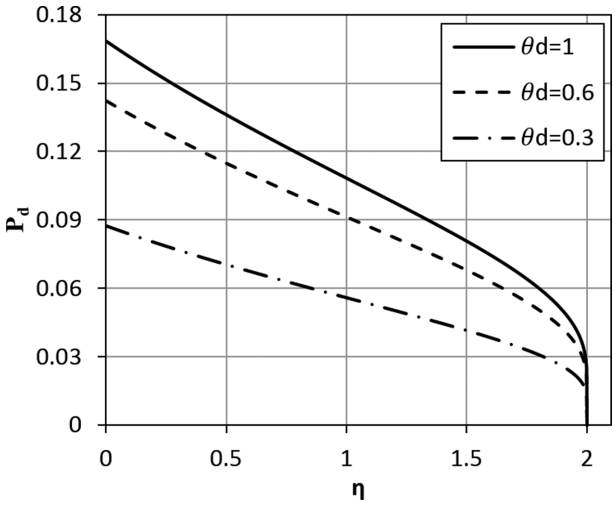

Fig. 4. Variations of the three local pressures with dimensionless curvature radius in permeate channel.

creasing the surface curvature leads to a decrease in pressure in the permeate channel, with the maximum decrease at the end of the channel closure. The dimensionless pressure distribution is flattened closer to the constant pressure with the higher degree of the surface curvature. Therefore, the assumption of the constant pressure in the permeate channel, which is commonly used in the literature, has the highest error in SWMs with low curvature. This con-

cept is apparent in Fig. 4, which shows the variations of the pressure at three different points across the channel width. According to the mathematical interpretation, the increase in surface curvature has led to a decrease in the parameter of B (as discussed previously), which indicates a decrease in the hydrodynamic relationship between the permeate channel and the feed channel. In which case the distribution of pressure in the permeate channel gets closer to the constant pressure distribution.

Fig. 5 and Fig. 6 show the distribution of pressure and the effect of surface curvature on the pressure in three points along the membrane length in the feed channel, respectively. According to the boundary conditions, the dimensionless pressure normalized by the p_{in} is 1 at the channel inlet and in the outlet is p_{od} which is equal to 0.9715 for the basic case study. The very small slope of the lines in Fig. 6 at points z_d=0.3 L_{xd} and z_d=0.6 L_{xd} shows the very small effect of surface curvature on the distribution of the feed channel pressure even at the exaggerated magnitudes of the dimensionless curvature radii. Therefore, one line is plotted for the pressure distribution of feed channel in Fig. 5, since it is almost independent of the curvature.

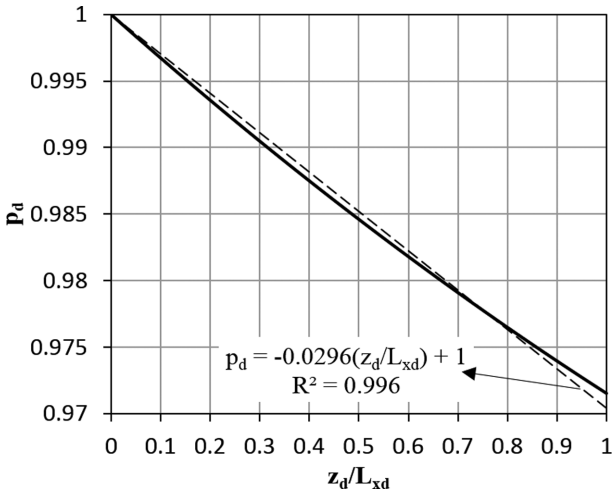

Fig. 5. Pressure distribution in feed channel.

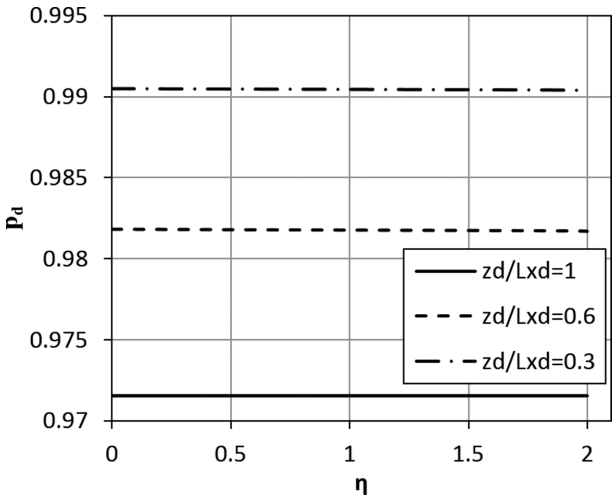

Fig. 6. Variations of the three local pressures with dimensionless curvature radius in feed channel

Note that in the model, the main flow direction of the water in the feed channel is considered only in *z*-direction so the flow does not feel curvature in its path geometrically. In which case, the very low dependency of the pressure on the surface curvature can be justified. Since the assumption of the single-dimensional flow of the meso/membrane scale in the feed channel is not far from the reality, it is not expected that two- or even three-dimensional flow solutions will significantly differentiate the effect of surface curvature on the pressure distribution of the feed channel.

Continuation of the inspection of Fig. 5 and focusing on the near-linear behavior of the figure, it is important to note that despite the simplifying assumption of the linear Darcy pressure equation in the process of the solution, the pressure curve is obtained close to linear pressure distribution but not exactly linear. The nonlinearity of the final pressure drop is interpreted by the complexity of the geometry of the spacers, which was implemented by the coefficient f_2 in dimensionless parameters of A and B.

3. Effect of the Surface Curvature on the Main Output Parameters

Using the analytical model developed in this paper, the impact of the main functional parameters of the RO SWM element from the membrane curvature can be studied. This effect is shown for the three main output parameters of the fluid recovery fraction (F), permeate flow rate (Q) and permeation flux in Fig. 7 by the percentage of difference ($\psi_{q,\eta}$). For example, as can be seen in Fig. 7, in the case with a constant dimensionless curvature radius of 0.5, the two parameters of the permeate water flow rate and the permeation flux are predicted 3.2% higher than their predicted values with the flat membrane assumption. This difference between the two solutions is 2.3% for the fluid recovery fraction. As it was predictable, the percentage of difference is greater at higher curvature radii. This difference increases linearly until the dimensionless curvature radius of 1.5 and then increases with a further slope. Note

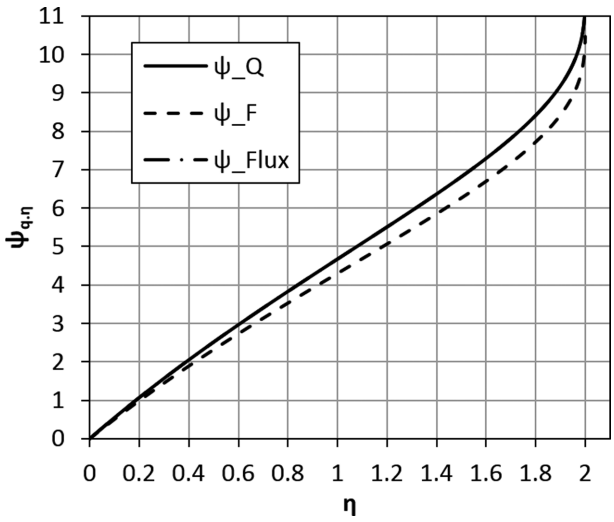

Fig. 7. The percentage of difference for the parameters of recovery fraction, permeate flow rate and permeation flux as the function of the dimensionless curvature radius.

that the overlapping of the lines for Q and flux is reasonable since the membrane dimensions in this graph are constant.

In general, the effect of the membrane curvature on the permeate flow rate is higher than the fluid recovery fraction, but for practical RO elements with dimensionless curvature radius less than 0.2, this difference is negligible, which for the basic case study is observed less than 1%. Note that this parameter would not be logically the same in the case of different applications such as ultrafiltration and nanofiltration.

Here, a point to be considered is that the percentage of difference between the results of the flat and the curved flow channels is not necessarily constant in a specified dimensionless curvature radius. For example, if the percentage of difference $\psi_{q,\eta}$ for η=0.15 is estimated at about 0.8% in Fig. 7, this value can be increased under the different physical parameters. To investigate this, three parameters of the membrane width (L_y), permeate channel permeability parallel to the membrane (k_1) and membrane resistance (R_m) are considered in Fig. 8 and Fig. 9 to show the percentage of difference variations for permeate flow rate and recovery fraction, respectively. These three physical parameters were selected because they can change the scale of B in the equations.

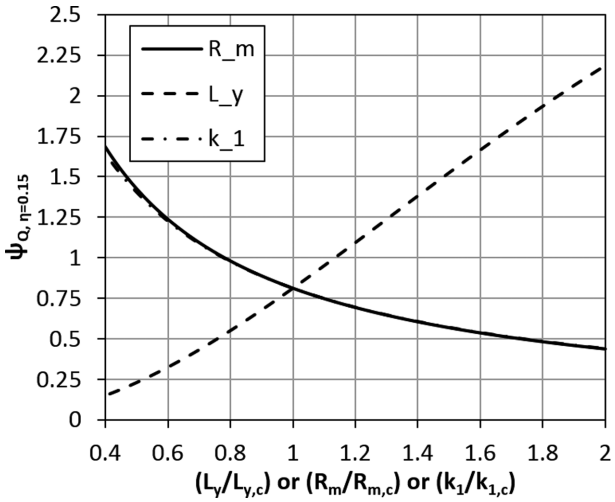

Fig. 8. The percentage of difference for the permeate flow rate at the dimensionless curvature radius of 0.15 as the function of the parameters L_y, R_m and k_1.

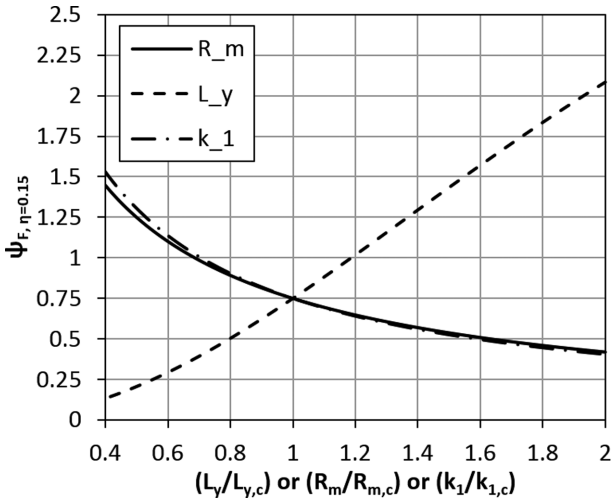

Fig. 9. The percentage of difference for the fluid recovery fraction at the dimensionless curvature radius of 0.15 as the function of the parameters L_y, R_m and k_1.

The physical parameters on the *x*-axis in Fig. 8 and Fig. 9 are normalized by the values of these quantities for the selected case study represented in Table 1 and are subscribed by c, for example, $L_{y,c}$=1.285 m. ψ_Q and ψ_F are also calculated in the dimensionless curvature radius of η=0.15 and in the form of $\psi_{Q,\eta=0.15}=(Q|_{\eta=0.15}-Q|_{Flat})/Q|_{Flat}\times100$ and $\psi_{F,\eta=0.15}=(F|_{\eta=0.15}-F|_{Flat})/F|_{Flat}\times100$. The observed trend in these two figures will be similar for the other values of the η, but the range of its values in the *y*-axis varies depending on the magnitude of the η. As can be seen, both figures have the same trend, but the percentage of difference for the fluid recovery fraction (Fig. 9) is slightly less than the permeate flow rate (Fig. 8).

The percentage of difference $\psi_{q,\eta=0.15}$ variability by the three physical quantities of L_y, k_1, and R_m is clearly visible in Fig. 8 and Fig. 9. For the selected case study, when the membrane resistance was reduced as much as 60% of the basic case value ($R_m/R_{m,c}$=1), the effect of the surface curvature more than doubled from 0.8% to about 1.7%. Thus, by decreasing the hydraulic resistance of the membrane located between the two flow channels (increasing the dimensionless value of B), the influence of the two channels from each other will increase, so the effect of the surface curvature in the solution would be more evident.

The same trend is also observed in the percentage of difference variation with the permeate channel permeability k_1. As an explanation, when the permeability of the porous medium in the permeate channel decreases, the resistance through the fluid flow will be increased so the distribution of the permeate channel pressure becomes more non-uniform. Since the pressure in the permeate channel is the function of θ which is closely related to the curvature, this non-uniformity of pressure is expected to increase the curvature effect to the output parameters, which is observed in the figures.

In the case of the membrane width parameter, the effect of surface curvature is increased with increasing membrane width in Fig. 8 and Fig. 9. Due to the fact that the surface curvature is felt by the fluid in the permeate channel along the width of the membrane, so an increase in the effect of surface curvature is expected as the membrane width increases.

4. Impact of the Surface Curvature on the Membrane Dimensions Corresponding to the Maximum Permeate Flow Rate

In the previous study [7], the main output parameters of the system could be theoretically maximized at the certain dimensions of the membrane. In this section, this concept is analyzed in Fig. 10 to Fig. 15 using the current solution model, including the effect of the surface curvature. Note that in this section, the output parameters have been evaluated with the selected case study geometric and operational parameters, while the length or width of the membrane is varying. Note that since the curvature of the surface is more effective along the width of the membrane, therefore, the results from Fig. 10 to Fig. 12 (which are relative to the membrane width) are quite different from the results with flat membrane

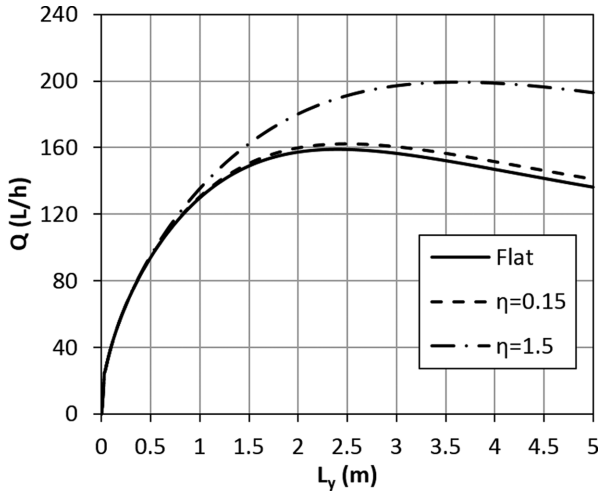

Fig. 10. Variation of permeate flow rate by membrane width with different dimensionless curvature radii.

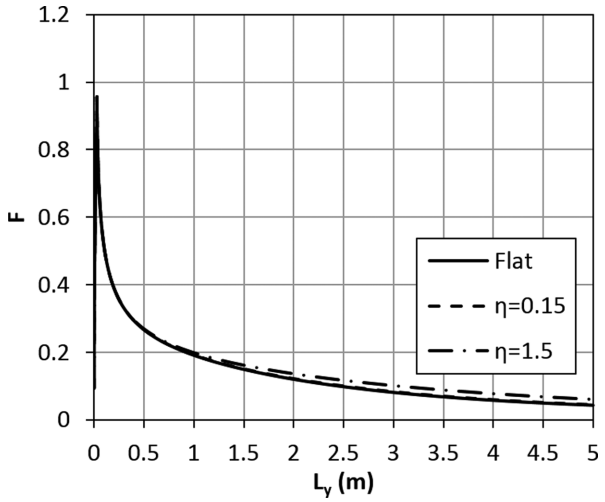

Fig. 11. Variation of fluid recovery fraction by membrane width with different dimensionless curvature radii.

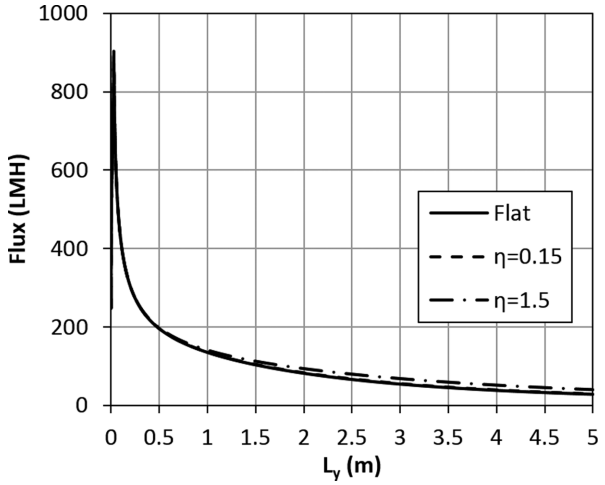

Fig. 12. Variation of permeation flux by membrane width with different dimensionless curvature radii.

assumption [7]. But this difference is less observed in the results of Fig. 13 to Fig. 15 that are relative to the membrane length.

According to Fig. 10 to Fig. 12, there is still a particular membrane width with maximum output parameters. Fig. 11 and Fig. 12 offer a very small membrane width for maximum fluid recovery and maximum permeation flux. Thus, they predict a reduction of recovery fraction and permeation velocity by increasing the width of the membrane. But differently, Fig. 10 shows that the maximum produced water flow rate for low curvatures for the selected case study, can be found within a membrane of about 2.3 to 2.5 m width, which may be inaccessible in reality.

It is observed that as the dimensionless radius of the curvature increases, the membrane width with maximum permeate water flow rate is increased too. But the curvature will not affect the width of the membrane with maximum fluid recovery fraction and maximum permeation flux. Also, in membrane widths less than about 0.7 m, the surface curvature does not affect the output parameters, but in elements with the higher membrane width, the flat-

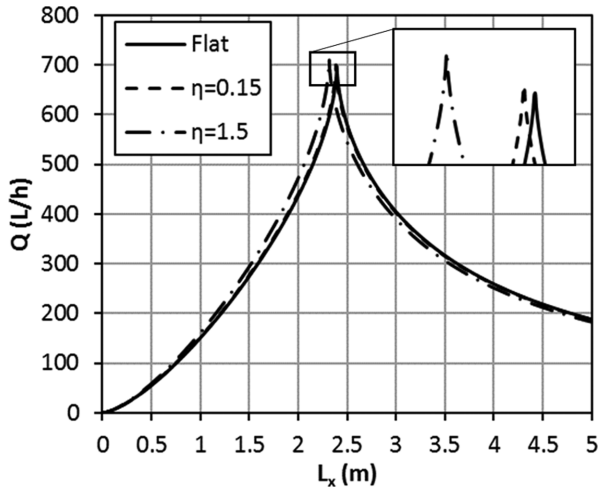

Fig. 13. Variation of permeate flow rate by membrane length with different dimensionless curvature radii.

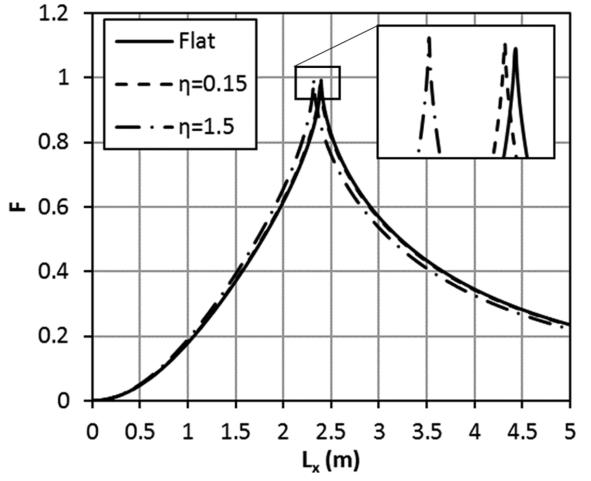

Fig. 14. Variation of fluid recovery fraction by membrane length with different dimensionless curvature radii.

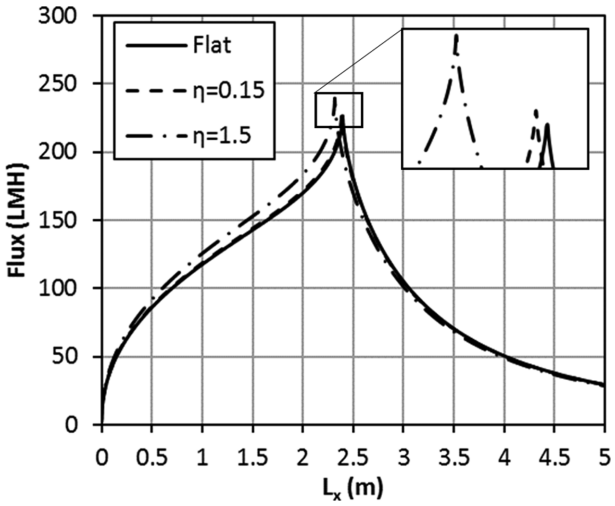

Fig. 15. Variation of permeation flux by membrane length with different dimensionless curvature radii.

sheet membrane assumption leads to a lower prediction of the output parameters than the curved membrane.

Fig. 13 to Fig. 15 also express the low surface curvature effect on the membrane length location and value with maximum output parameters. As can be seen, only in the exaggerated dimensionless curvature radius of 1.5 is a slight difference observed at the absolute extrema of the graph, and the difference made by low surface curvatures is very small. In this analysis, the length of the membrane with the maximum output parameters was calculated to be about 2.3 to 2.4 m, which may not be possible in practice today.

CONCLUDING REMARKS

An analytical model to represent the hydrodynamics of fluid flow in SWMs has been developed and implemented for a reverse osmosis water treatment element. The pursued line had two main achievements. First, the new model was introduced under a more realistic geometry condition included the surface curvature. Second, this approach led to having the capability of analyzing the effect of the membrane curvature mathematically. Thus, the accuracy of the commonly used assumption of flat-sheet membrane can be investigated in wider geometric and operational conditions with lower computational cost in comparison with numerical studies.

The influences of the curvature on the feed and permeate channels pressure and on the main output parameters of permeate water flow rate, fluid recovery fraction and permeation flux were investigated with the fixed and variable membrane dimensions. It was found that the three physical parameters of the membrane width (L_y), the permeate channel permeability parallel to the membrane (k_1) and the membrane resistance (R_m), can increase the difference between the predicted value of the output parameters in the solution with the flat and curved membrane even several times. This issue was examined in an element with the fixed curvature radius to focus on the increasing effect of these three parameters. So the value of these parameters should be taken into account in studies that assume the flat membrane. Another significant effect of the curvature on the permeate channel pressure distribution was observed. In addition, the effect of the membrane width variation on output parameters in the current model was obtained completely different from the previous one with flat membrane assumption. In the selected reverse osmosis element, it was estimated that the permeate water flow rate will reach its maximum theoretical level in the membrane with a width of about 2.3 m (assuming a constant membrane length) and also in a membrane with a length of about 2.4 m (assuming a constant membrane width).

Although some undeniable curvature effects were observed, they can be ignored in some cases. For example, in the selected case study, which was a reverse osmosis element, the percentage of difference for the output parameters was found to be less than 0.8% within the real range of the curvature with η<0.15.

NOMENCLATURE

A, B, C : dimensionless parameters defined in the model
D : diameter of the feed spacer filament [m]
F : fluid recovery fraction
f_1, f_2 : coefficients in pressure drop constitutive law (feed channel)
k : permeability [m^2]
k_1 : permeate channel permeability parallel to the membrane [m^2]
k_2 : permeate channel permeability perpendicular to the membrane [m^2]
L : length of the feed spacer filament in a unit cell [m^2]
L_{pr} : permeate channel height [m]
L_{fr} : feed channel height [m]
L_x : membrane sheet length [m]
L_y : membrane sheet width [m]
LMH : permeation flux [L/(m^2 h)]
P : permeate channel pressure [Pa]
p : feed channel pressure [Pa]
Q : permeate flow rate [L/h]
R : curvature radius [m]
R_m : membrane resistance [m^{-1}]
Re : Reynolds number (Re=ρUD/μ)
U : velocity in feed channel [m/s]
U_w : permeation velocity or permeation flux [m/s]

Greek Symbols

Θ : angle corresponds to the membrane width [Deg]
η : dimensionless curvature radius
ψ : percentage of difference [%]
α : dimensionless parameter defined in the solution
β : mesh angle (between the filaments of feed spacer) [Deg]
ΔP : pressure drop [Pa]
μ : fluid viscosity [Pa·s]
ρ : fluid density [kg/m^3]

Subscripts

c : related to selected case study value
d : dimensionless
in : inlet
out : outlet

i : inner
o : outer
f : related to feed channel
p : related to permeate channel
r : index notation for cylindrical coordinates
θ : index notation for cylindrical coordinates
z : index notation for cylindrical coordinates
q : quantity (main output parameter)

REFERENCES

1. S. Homaeigohar and M. Elbahri, *NPG Asia Mater.*, **9**(8), e427 (2017).
2. M. Elimelech and W. A. Phillip, *Science*, **333**(6043), 712 (2011).
3. A. H. Haidari, S. G. J. Heijman and W. G. J. van der Meer, *Sep. Purif. Technol.*, **192**, 441 (2018).
4. H. S. Abid, D. J. Johnson, R. Hashaikeh and N. Hilal, *Desalination*, **420**, 384 (2017).
5. C. Bae, K. Park, H. Heo and D. R. Yang, *Korean J. Chem. Eng.*, **34**(3), 844 (2017).
6. D. Lin, Z. Ding, L. Liu and R. Ma, *Comput. Chem. Eng.*, **44**, 20 (2012).
7. M. Taherinejad, S. Derakhshan and A. Yavarinasab, *Desalination*, **411**, 59 (2017).
8. A. H. Haidari, S. G. J. Heijman and W. G. J. van der Meer, *Sep. Purif. Technol.*, **199**, 9 (2018).
9. A. I. Radu, M. S. H. van Steen, J. S. Vrouwenvelder, M. C. M. van Loosdrecht and C. Picioreanu, *Water Res.*, **64**, 160 (2014).
10. S. S. Hong, W. Ryoo, M.-S. Chun and G.-Y. Chung, *Korean J. Chem. Eng.*, **32**(7), 1249 (2015).
11. B. Gu, C. S. Adjiman and X. Y. Xu, *J. Membr. Sci.*, **527**, 78 (2017).
12. A. Siddiqui, S. Lehmann, V. Haaksman, J. Ogier, C. Schellenberg, M. C. M. van Loosdrecht, J. C. Kruithof and J. S. Vrouwenvelder, *Water Res.*, **119**, 304 (2017).
13. C. P. Koutsou, A. J. Karabelas and M. Kostoglou, *Sep. Purif. Technol.*, **147**, 90 (2015).
14. M. Kostoglou and A. J. Karabelas, *Ind. Eng. Chem. Res.*, **48**(22), 10025 (2009).
15. D. Y. Kim, B. Gu and D. R. Yang, *Korean J. Chem. Eng.*, **30**(9), 1691 (2013).
16. O. Kavianipour, G. D. Ingram and H. B. Vuthaluru, *J. Membr. Sci.*, **526**, 156 (2017).
17. M. Li, T. Bui and S. Chao, *Desalination*, **397**, 194 (2016).
18. V. V. Ranade and A. Kumar, *J. Membr. Sci.*, **271**(1-2), 1 (2006).
19. Y. Li and K. Tung, *J. Membr. Sci.*, **319**(1-2), 286 (2008).
20. Y. L. Li, K. L. Tung, M. Y. Lu and S. H. Huang, *J. Membr. Sci.*, **329**(1-2), 106 (2009).
21. Y. L. Li, K. L. Tung, Y. S. Chen and K. J. Hwang, *Desalination*, **287**, 200 (2012).
22. S. Wardeh and H. P. Morvan, *Desalination and Water Treatment,* **1**(1-3), 277 (2009).
23. K. L. Tung, H. C. Teoh, C. W. Lee, C. H. Chen, Y. L. Li, Y. F. Lin, C. L. Chen and M. S. Huang, *J. Membr. Sci.*, **495**, 489 (2015).
24. A. J. Karabelas, M. Kostoglou and C.P. Koutsou, *Desalination,* **356**, 165 (2015).
25. M. Taherinejad, J. Gorman, E. Sparrow and S. Derakhshan, *J. Membr. Sci.*, **563**, 210 (2018).
26. C. P. Koutsou, S. G. Yiantsios and A. J. Karabelas, *J. Membr. Sci.*, **291**(1-2), 53 (2007).
27. P. Sousa, A. Soares, E. Monteiro and A. Rouboa, *Desalination*, **349**, 22 (2014).
28. M. Kostoglou and A. J. Karabelas, *Desalination*, **316**, 91 (2013).
29. M. B. Minhas and W.-S. Kim, *Desalination and Water Treatment*, **54**(9), 2343 (2014).
30. P. P. Mane, P. K. Park, H. Hyung, J. C. Brown and J. H. Kim, *J. Membr. Sci.*, **338**(1-2), 119 (2009).
31. H. Boulahfa, S. Belhamidi, F. Elhannouni, M. Taky, A. El Fadil and A. Elmidaoui, *J. Environ. Chem. Eng.*, **7**(2), 102937 (2019).